

# We are IntechOpen, the world's leading publisher of Open Access books Built by scientists, for scientists

6,900

Open access books available

186,000

International authors and editors

200M

Downloads

Our authors are among the

154

Countries delivered to

TOP 1%

most cited scientists

12.2%

Contributors from top 500 universities



WEB OF SCIENCE™

Selection of our books indexed in the Book Citation Index  
in Web of Science™ Core Collection (BKCI)

Interested in publishing with us?  
Contact [book.department@intechopen.com](mailto:book.department@intechopen.com)

Numbers displayed above are based on latest data collected.  
For more information visit [www.intechopen.com](http://www.intechopen.com)



# Surgical Planning and Additive Manufacturing of an Anatomical Model: A Case Study of a Spine Surgery

*Levent Aydin, Ozgur Cakir, Riza Dilek and Mucahit Ege*

## Abstract

3D scanning technologies have promising solutions for medical needs such as anatomical models, biocompatible implants, and orthotic/prosthetic models. Although virtual presurgical planning offers more precise results, it may not be applied in every hospital because of the high costs. The aim of this study is to assess the accuracy of the suggested low-cost and effective surgical planning method by means of additive manufacturing to increase success rate of each surgery. In this study, a full spine model of a scoliosis patient was acquired and reconstructed in MIMICS software using different filters and parameters. Therefore, a comparison in terms of geometrical errors among each model was performed based on a reference model. Subsequently, patient-specific full spine model was manufactured using a three-dimensional printing method (fused deposition modeling) and utilized before the surgery. 3D surgical model reconstruction parameters such as wrap tool, binomial blur, and curvature flow filters produced high geometrical errors, while mean filter produced the lowest geometrical error. Furthermore, similarity results of the curvature flow and discrete Gaussian filters were close to mean filter. Smooth tool and mean filter produced almost the same volume of the reference model. Consequently, an ideal protocol for surgical planning of a spine surgery is defined with measurable accuracy. Thus, success rate of a spine surgery may be increased especially for the severe cases owing to the more accurate preoperative review: operability.

**Keywords:** additive manufacturing, image guided surgery, orthopedic surgery, surgical planning, accuracy assessment, scoliosis

## 1. Introduction

Scoliosis is a three-dimensional (3D) deformity in the natural shape of spine that requires surgery in serious cases [1]. A lateral deviation of the spine greater than 10 degrees is accepted as scoliosis and an abnormal sideways curvature is observed from the frontal plane of a patient, while a healthy spine should look like straight [2, 3]. Although hereditary factors play a role in the etiology, most of the cases (80% of the patients) with unknown cause are called idiopathic scoliosis and classified into three main groups based on the age, namely, (i) infantile (up to 3 years

old), (ii) juvenile (4–9 years old), and (iii) adolescent (10 years old to teen years) [4]. The severity of scoliosis is also determined by Cobb method that provides obtain information about the curvature of the spine in terms of degrees. According to these measurements, a scoliotic curve of the spine is defined as (i) mild scoliosis (10–25°, requires monitoring), (ii) significant scoliosis (25–40°, treated with bracing), and (iii) severe scoliosis (over 40°, requires surgery) [5]. Recently, a number of the scoliosis patients are growing up to 2–3% worldwide due to the unawareness of people [6]. It is important to predict risk of progression, diagnose at early stage for preventing degenerative effects, and contribute to the patient's quality of life. Unfortunately, in some cases, rapid progress on spine deformity or late diagnosis is resulted with surgical operations that are necessary to stabilize the spine by means of rod placement on each affected vertebra [6]. All operations require precise processes in a limited workspace because of the spinal nerves and blood vessels. Besides, an injury of a vessel around the surgical site may initiate clotting that may result with pulmonary embolism or even death [7]. Therefore, novel technologies and methods are of great importance to assist or plan the surgery in advance.

Medical imaging technologies such as multidetector computed tomography (MDCT) and magnetic resonance imaging (MRI) are rapidly evolving to visualize more complex tissues of the human body [8]. Furthermore, high-resolution images provide radiologists more accurate diagnosis [9]. Although 3D visualization of the scanned tissues simplifies the surgical procedures, patients may undergo a suboptimal outcome after the treatment [10]. On the other hand, two-dimensional (2D) computer screens prevent the direct interaction with the target 3D model [11]. While virtual presurgical planning offers more precise results and overcomes mentioned drawbacks above, it is not applicable for every hospital because of its high costs [10]. Additive manufacturing, layer-by-layer fabrication of a physical object, is increasingly being used especially in the fields of medicine. Nowadays, these technologies are utilized with medical imaging to produce patient-specific (i) medical devices, orthosis, and prosthesis [12], (ii) anatomical to assist-surgical models [13], (iii) body parts [14], (iv) dental and maxillofacial implants [15], (v) blood vessels [16], and (vi) organs [17]. Typical 2D digital imaging and communications in medicine (DICOM) files from the CT or MRI images are transformed into a 3D standard tessellation language (STL) file to perform 3D printing of the target model. A wide range of polymers including glass, ceramic, metal, or biological materials may be used to create complex models in a cost-effective way compared to conventional manufacturing methods [18]. Although the latest innovative studies are focused on a functional tissue or even an organ printing, clinical bedside applications of these technologies are difficult and limited [11]. On the other hand, surgical planning or patient-specific implant production via 3D printing is available for any case and widely used to manage a complex surgery or achieve the exact placement of an implant [18]. Consequently, success rate of each surgery is significantly increased as well as it becomes minimally invasive and requires shorter recovery owing to the preoperative review [19, 20].

Surgical planning by means of additive manufacturing consists of five basic steps, namely, (i) data acquisition, (ii) image segmentation, (iii) 3D model reconstruction, (iv) 3D printing, and (v) preoperative review [21]. In data acquisition step, a medical imaging system such as CT is used to obtain 2D DICOM images in general. The accuracy of surgical planning is first dependent on the contrast-to-noise ratio (CNR) of scanned raw images [22]. High CNR values provide detailed segmentation before the 3D reconstruction of a model. These images are then processed via a commercial (Materialize Mimics) or an open-source (InVesalius) medical image processing software using the default segmentation functions or manual

selection of the region of interest on each image during the segmentation step. Thus, the target anatomical model's contour is masked on each image section. In 3D model reconstruction step, the mask images are positioned sequentially to form a solid model in 3D workspace of the software. Tissue-specific filters or data sets may be applied to minimize noise using predefined thresholds before and after the 3D reconstruction process. The solid model is exported as a STL file and prepared to be 3D printed. In 3D printing step, the STL file is 3D printed using one of the additive manufacturing methods such as fused deposition modeling (FDM), selective laser sintering (SLS), or stereolithography (SLA). In a preoperative review step, the printed model is evaluated and used before and during the surgery (requires sterilization) as a reference model that guide the operation as well as it can be used for custom implant or assistive surgical apparatus creation such as drill guides [23]. Since surgical planning is important and plays a crucial role during the surgery, reference 3D model requires to be created with minimal geometrical errors. The accuracy of 3D reconstructed models can be analyzed by calculating the Hausdorff distance (HD) and dice similarity coefficient (DSC) values for each model [24, 25]. While DSC measures the volume overlap between two models that ranges from 0 (no overlap) to 1 (exact overlap), HD calculates the Euclidean distance between each binary volume [26, 27]. Furthermore, several methods (geometric distance, roughness, structure, saliency, and strain-energy-based calculations) may be implemented to assess visual quality and accuracy of the 3D models [28]. In this study, a spine model of a scoliosis patient is first acquired and then 3D reconstructed in MIMICS software (manual and automatic segmentation) using different filters and parameters to compare each geometrical error. The results of the DSC and HD values of each reconstructed model reveal the ideal protocol for surgical planning of a spine surgery and determine the accuracy of the created model.

## 2. Material and methods

A 6-year-old patient (male) who has a congenital scoliosis history participated to this study for obtaining raw image data. Medical scanning process was performed at the Radiology Department, Faculty of Medicine Kocaeli University, using a CT scanner (Aquillion 64, Toshiba Medical Systems, Tokyo, Japan). Ethical permission was received by the Ethics and Research Committee of Kocaeli University (reference number, KU GOKAEK 2019/204). A full spinal CT scanning was performed at 2 mm of slice thickness, 140 mm field of view (FoV) and 135 kV (40 mA, 1 s). Raw DICOM images (449 slices) were obtained from the picture archiving and communication system (PACS) server of the Radiology Department (**Figure 1(a)**). Thus, data acquisition process, the first step of the surgical planning, was completed.

MIMICS software (v19) was utilized in image segmentation step, and a reference model was automatically reconstructed via MIMICS without any filters (**Figure 1(b)**). DICOM files (449 images) were imported, and segmentation process was performed using the thresholding tool at predefined threshold set of the bone (226, Hounsfield Unit, HU as lower threshold, and 3071 HU as higher threshold). These parameters were ideal to obtain exact contour of the target model in a maximum allowable noisy form according to the raw DICOM images for this case. Segmentation step was completed after each image section was masked and highlighted by a different color (**Figure 1(c)**).

3D calculation function was utilized at high quality to reconstruct the 3D raw surface, and a quite noisy model was created with desired contour based on the masked images in 3D model reconstruction step (**Figure 1(d)**). Each image

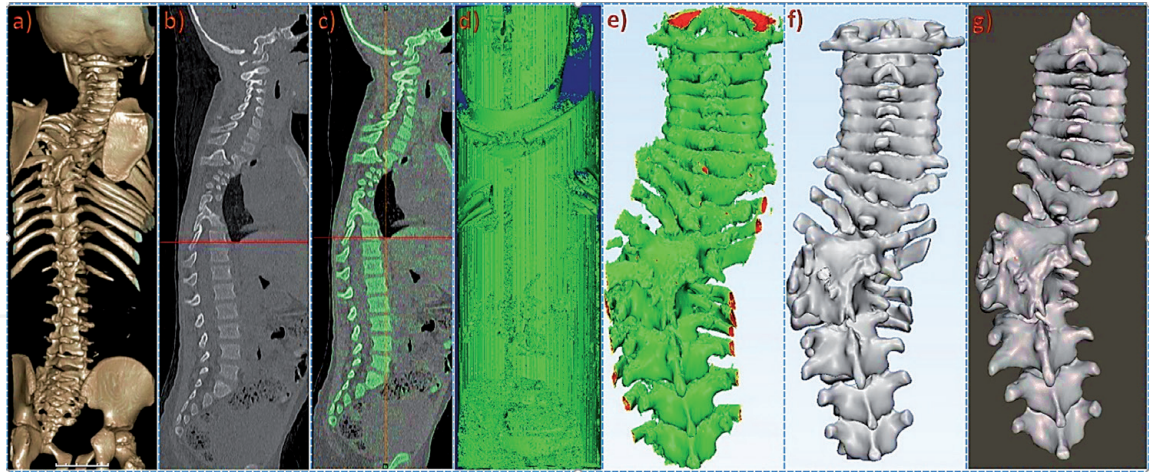


**Figure 1.** 3D Surgical model segmentation of the reference model (a) An image of the 3D raw model, based on non-filtered DICOM images in Sectra workspace, a 3D DICOM viewer of the default system software that does not allow 3D model exporting or processing, (b) Importing non-filtered DICOM images in MIMICS, (c) Segmentation of each image and obtaining the exact contour of target model in a maximum allowable noisy form in MIMICS, (d) 3D reconstruction of the raw DICOM images in a noisy form via MIMICS, (e) Manual noise cleaning in 3-Matic, (f) Manual surface reconstruction and fixing the geometrical errors of 3D raw model in 3-Matic, (g) Fixing the sharp cornered bonded surfaces in Meshmixer.

was positioned sequentially to form a 3D raw model of the spine. Since there was noise in the workspace and model's surface, the 3D raw model was directly exported to 3-matic software (v11, Materialize) for manual surface reconstruction and noise elimination (**Figure 1(e)**). The surface geometry of the model was manually revised, and the noise was manually cleared via 3-matic software according to the raw image geometries in MIMICS. Polygon area mark tool under the Mark—Area Mark menu was used to select each noisy surface and subsequently deleted. The gaps of the deleted surfaces were marked as bad contours on the 3D raw model. The bad contours were then selected and fixed, respectively, using the Fill Hole Freeform tool under the Fix menu. The Fill Hole Freeform process was performed at medium triangulation quality and created in tangent form. After manual surface reconstruction, the Fix Wizard tool under the Fix menu was utilized to fix geometrical normals, stitching, noise shells, holes, triangles, overlaps, and shells on the model. The errors were automatically fixed by clicking Follow Advice, Apply, and Update buttons, respectively, for each option (**Figure 1(f)**). Finally, the patient ID was added using the Quick Label tool under the Finish menu. Thus, 3D-reconstructed reference surgical model was obtained and exported as STL file by clicking File, Export, and STL buttons, respectively. The reference model was exported at binary format and one scaling factor. Some sharp cornered bonded surfaces that occurred by Fix Wizard tool during the fixing process were also revised in Meshmixer (v3.4.35, Autodesk) manually to obtain exact geometry of target anatomical model. Robust Smooth tool under the Sculpt – Brushes menu was used (brush parameters, 10 strength, 10 size, 0 depth, and 0 laziness) to fix sharp surfaces (**Figure 1(g)**). The 3D model reconstruction step was completed after the reference model has taken its final shape (48 hours of work). 3D reconstruction of the reference surgical model is illustrated step by step in **Figure 1**.

Test models were separated into three groups, namely, (i) preprocessed, (ii) post-processed, and (iii) fully processed models. Preprocessed models were obtained using the filtered DICOM images before the segmentation step without any post-process in MIMICS. Post-processed models were created from the raw DICOM images and only processed via 3-matic after the model was

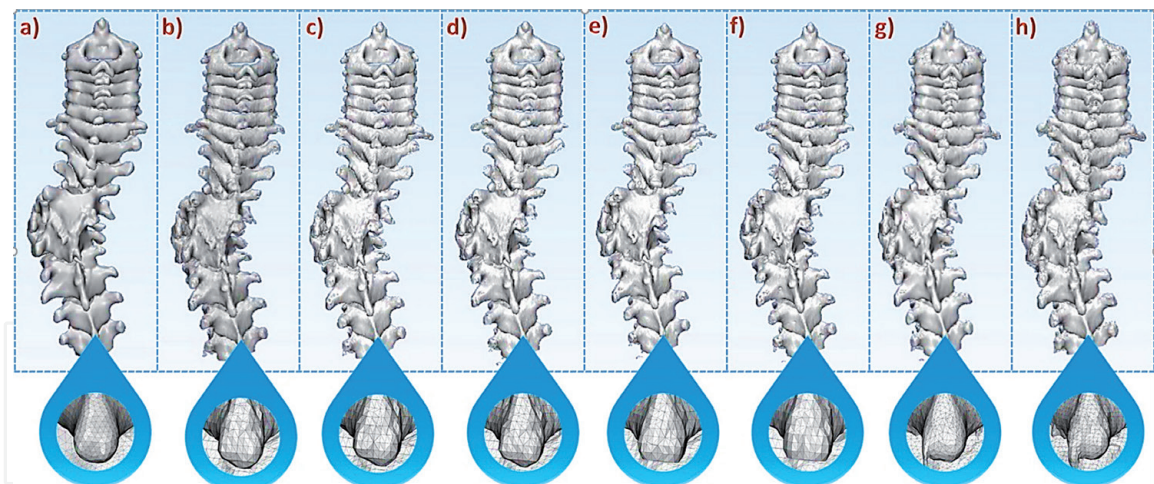


**Figure 2.** Reference model and each generated 3D test model with a local mesh view (a) Reference model, (b) Binomial blur filter in MIMICS, (c) Curvature flow filter in MIMICS, (d) Discrete gaussian filter in MIMICS, (e) Mean filter in MIMICS, (f) Median filter in MIMICS, (g) Smooth function in 3-Matic and (h) Wrap function in 3-Matic.

reconstructed (**Figure 2(a)**). Fully processed models were formed with a combination of both processes. Five different image filters of MIMICS, (i) binomial blur (**Figure 2(b)**), (ii) curvature flow (**Figure 2(c)**), (iii) discrete Gaussian (**Figure 2(d)**), (iv) mean (**Figure 2(e)**), and (v) median (**Figure 2(f)**), were applied on the raw DICOM images, respectively, and then the segmentation step was performed separately for each sample on preprocessed models. Two different 3D tools of 3-matic, (i) Smooth (**Figure 2(g)**) and (ii) wrap (**Figure 2(h)**), were utilized separately for each sample in post-processing case. Preprocessing, post-processing, and full-processing parameters of the 3D reconstructed surgical models are given in **Table 1**.

Before the calculation of HD and DSC values by CloudCompare software, each spine model was processed via 3-matic software that was necessary to determine the spine regions equally on each sample model and obtain more correct results in accuracy assessment. Therefore, the spine sections of each model were extracted manually and exported using the default options. All test models were imported into the CloudCompare software (v2.11, Open Source) and then compared with the reference model in terms of the HD and DSC results [29]. The best results of the preprocessing and the post-processing cases were combined and applied together to form the fully processed model. Finally, the fully processed model was compared to the reference model to reveal the ideal solution for 3D surgical model reconstruction. Each generated test model is illustrated in **Figure 2**.

HD of the test models was calculated by means of importing and analyzing the 3D models, the reference model and one of the test models at the same time, in CloudCompare workspace. Both models were then aligned using Registration Match bounding function—under the Tools menu. This process is required to align the box centers (volume frames) of models before performing any similarity function in order to obtain accurate results. Fine registration function under the Tools—Registration menu was applied on each model to highlight the difference of point clouds without any scale adjustment. The fine registration function also applies a rotation to compared model (generates a rotation matrix with a theoretical overlap value) to provide an ideal Overlap in volumes of the both reference and compared test model. Finally, HD value (mean distance) was computed via Distances—Cloud/Mesh Dist under the Tools menu. DSC values were calculated similarly via importing

Pre-processing parameters of applied filters in MIMICS			
Model no.	Filter name	Parameter	Value
1	Binomial blur	Number of iterations	5
2	Curvature flow	Time step	0.5
		Number of iterations	5
3	Discrete Gaussian	Gaussian variance	5
		Max kernel width	5
4	*Mean	Filter radius	3
5	Median	Filter radius	3
Post-processing parameters of applied tools in 3-matic			
6	*Smooth	Smooth factor	1
7	Wrap	Gap closing	0.05
		Smallest detail	0.5
Full-processing parameters of both applied filter and tool			
8	*Mean with *Smooth together	Filter radius	3
		Smooth factor	0.5

(\* = best similarity results).

**Table 1.**  
Parameters of each applied filters and tools.

the reference model and a test model into the 3D workspace of CloudCompare software. The match bounding and fine registration steps were also performed to obtain perfect alignment. After the alignment process, a plugin named as Cork, under the Plugins menu, was utilized to obtain the intersection of both models in terms of volume (cube units). Each volume was also measured by means of the mesh measure volume function under the Edit menu. The DSC value of each model was then calculated to obtain overlapped volume between the two models according to the formula given below ( $\alpha$  = total volume of the reference model,  $\beta$  = total volume of the compared model, and  $\alpha \cap \beta$  = intersection of both models in terms of volume):

$$DSC(\alpha, \beta) = \frac{2(\alpha \cap \beta)}{\alpha + \beta} \quad (1)$$

### 3. Results

Wrap tool, binomial blur, and curvature flow filters produce high geometrical errors, while mean filter produces the lowest geometrical error. Furthermore, HD and DSC results of the curvature flow and discrete Gaussian filters are close to mean filter. Smooth tool and mean filter produce almost the same volume of the reference model. However, binomial blur filter and wrap tool generate unacceptably different volumes. Moreover, the DSC results of the both mentioned functions are not overlapping properly. Each result is illustrated in **Table 2**.

Smooth and wrap tools generate undesired mesh structures caused by the noise during the segmentation step in MIMICS. HD results of each test model are illustrated in **Figure 3**.

HD and DSC results of each test model						
No.	Filter-tool name	Filter type	Model volume (cube units)	Max error (%)	HD (mm)	DSC (0–1)
1	Binomial blur	Pre	80393.9	9.502507	1.083704	0.547654
2	Curvature flow	Pre	81445.2	8.31908	1.107846	0.923381
3	Discrete Gaussian	Pre	81787.5	7.933765	1.034391	0.911621
4	Mean	Pre	82308.1	7.347738	1.041506	0.913479
5	Median	Pre	79867.7	10.09483	1.043368	0.911775
6	Smooth	Post	90480.1	-1.851286	1.185564	0.937718
7	Wrap	Post	113,092	-27.30496	0.461971	0.871986
8	Mean + Smooth	Together	82231.4	7.434077	1.041154	0.916657

Reference model volume (cube units): 88835.5

**Table 2.**  
 Results of each applied filters and tools (DSC value: 0 = no overlap, 1 = exact overlap, negative max error values indicate a larger volume than the reference model while positive values mean a lower volume according to the reference model in terms of cube units).

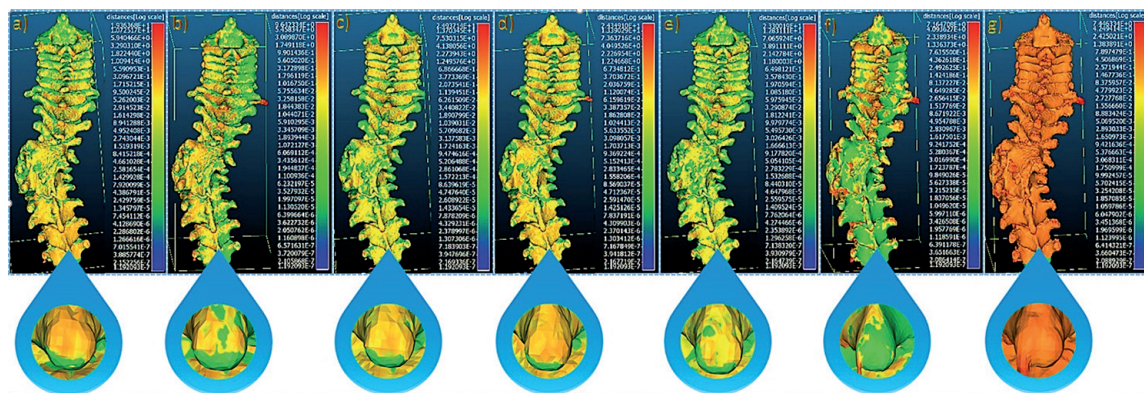


**Figure 3.**  
 The intersection of reference model and each generated 3D test model with a local view (a) Reference model and Binomial blur pre-filtered test model, (b) Reference model and Curvature flow pre-filtered test model, (c) Reference model and Discrete gaussian pre-filtered test model, (d) Reference model and Mean pre-filtered test model, (e) Reference model and Median pre-filtered test model, (f) Reference model and Smooth post-filtered test model and (g) Reference model and Wrap post-filtered test model.

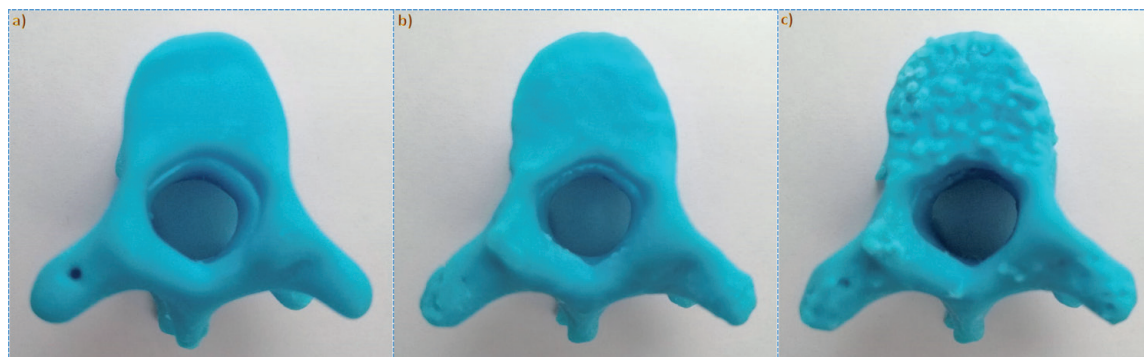


**Figure 4.**  
 Results of each produced model. (a) Reference model, (b) Mean filter and (c) Smooth tool.

The results of the last case given in **Table 2** (mean filter with Smooth tool together) show that increased Smooth provides to obtain better HD and DSC results when compared to the fourth test case (mean filter only). However, the max error is proportionally increased with the Smooth tool. Reference model, mean filter, and Smooth tool results are illustrated in **Figure 4**.

#### 4. Discussion

According to the results, binomial blur filter, median filter, and wrap tool are not suitable for surgical planning of a spine model due to the high error percentage in volume. These functions produce misleading information when used alone and may be used with another filter together at lower parametric values. Although Smooth tool provides better DSC result than the curvature flow filter, mesh surface improvement should not be performed by means of this tool only because of the undesired mesh structures caused by the noise. Therefore, a prefilter-like curvature flow, discrete Gaussian, or mean should be applied on raw DICOM images to filter noise more accurately during the segmentation step, and Smooth tool should be used at lower values after 3D model reconstruction process. It should be noted that some geometrical errors may not be fixed via 3-matic software and may require a third party software such as Geomagic Design X or Autodesk Meshmixer. On the other hand, fractured or unbounded bone structures may be lost during the noise filtering process. Therefore, some functions such as largest surface selection in MIMICS should not be used in complex cases, and target model should be cleared manually after the 3D reconstruction process. Mesh distribution of the models require to be uniform to perform a healthy DSC calculation. Both reference and compared test models may be processed via optimize mesh tool in Geomagic Design X to achieve uniform mesh distribution on each model.

While software optimizations may be performed to obtain an ideal protocol, improvements may also be applied on used CT device at the beginning for more correct presurgical planning. Devices with more advanced detector structure, which could provide to operate at lower voxels and have high beam quality, may reduce noise on raw data images. For example, it is known that dual energy computed tomography (DECT) is more suitable for tissue segmentation than single-energy computed tomography (SECT) [30]. Besides, some known sources of noise (beam hardening, partial volume effect, etc.) can be reduced by making some adjustments before imaging such as in monochromatic X-ray, reduced beam hardening effect and thin section thickness, and reduced the partial volume effect, which are very important for spine imaging [31, 32]. Additionally, using higher tube current provides sharper image because of the amount of beam delivery to the target tissue. However, high current may not be applied in all cases because of the increased radiation dose given to the patient.

#### 5. Conclusion

In this study, an ideal protocol for surgical planning of a spine surgery is defined with measurable accuracy. Thus, success rate of a spine surgery may be increased especially for the severe cases owing to the more accurate preoperative review.

#### Acknowledgements

We declare that we have no acknowledgments.

IntechOpen

### **Author details**

Levent Aydin<sup>1</sup>, Ozgur Cakir<sup>2</sup>, Riza Dilek<sup>3</sup> and Mucahit Ege<sup>1\*</sup>

1 Biomedical Device Technology, Istanbul Gedik University, Istanbul, Turkey

2 Department of Radiology, Faculty of Medicine, Kocaeli University, Kocaeli, Turkey

3 Medical Imaging Techniques, Istanbul Gedik University, Istanbul, Turkey

\*Address all correspondence to: [mucahit.ege@gedik.edu.tr](mailto:mucahit.ege@gedik.edu.tr)

### **IntechOpen**

© 2019 The Author(s). Licensee IntechOpen. This chapter is distributed under the terms of the Creative Commons Attribution License (<http://creativecommons.org/licenses/by/3.0>), which permits unrestricted use, distribution, and reproduction in any medium, provided the original work is properly cited. 

## References

- [1] Choudhry MN, Ahmad Z, Verma R. Adolescent idiopathic scoliosis. *The Open Orthopaedics Journal*. 2016;**10**:143
- [2] Scoliosis—Better Health Channel. 2019. Available from: [betterhealth.vic.gov.au/health/ConditionsAndTreatments/scoliosis?viewAsPdf=true](https://betterhealth.vic.gov.au/health/ConditionsAndTreatments/scoliosis?viewAsPdf=true) [Accessed: June 20, 2019]
- [3] Miller MD, Thompson SR, Hart J. Review of orthopaedics. Elsevier Health Sciences; 2012. p. 1
- [4] Treating Scoliosis. 2019. Available from: <https://www.treating scoliosis.com/infographics/scoliosis-by-the-numbers/> [Accessed: June 20, 2019]
- [5] Napierkowski DB. Scoliosis: A case study in an adolescent boy. *Orthopaedic Nursing*. 2007;**26**(3):147-155
- [6] Grauers A, Einarsdottir E, Gerdhem P. Genetics and pathogenesis of idiopathic scoliosis. *Scoliosis and Spinal Disorders*. 2016;**11**(1):45
- [7] University of Maryland School of Medicine. 2019. Available from: <https://www.umms.org/ummc/health-services/orthopedics/services/spine/patient-guides/complications-spine-surgery> [Accessed: June 20, 2019]
- [8] Rengier F, Mehndiratta A, Von Tengg-Kobligk H, et al. 3d printing based on imaging data: Review of medical applications. *International Journal of Computer Assisted Radiology and Surgery*. 2010;**5**(4):335-341
- [9] Kido T, Kurata A, Higashino H, et al. Cardiac imaging using 256-detector row four-dimensional CT: Preliminary clinical report. *Radiation Medicine*. 2007;**25**(1):38-44
- [10] Palau JR. Three-dimensional planning in craniomaxillofacial surgery. *International Journal of Oral and Maxillofacial Surgery*. 2017;**46**:46
- [11] Chae MP, Rozen WM, McMenamain PG, et al. Emerging applications of bedside 3d printing in plastic surgery. *Frontiers in Surgery*. 2015;**2**:25
- [12] Aydin L, Kucuk S. A method for more accurate fea results on a medical device developed by 3d technologies. *Polymers for Advanced Technologies*. 2018;**29**(8):2281-2286
- [13] Kurenov SN, Ionita C, Sammons D, et al. Three-dimensional printing to facilitate anatomic study, device development, simulation, and planning in thoracic surgery. *The Journal of Thoracic and Cardiovascular Surgery*. 2015;**149**(4):973-979
- [14] Wallace GG, Cornock RC, O'Connell CD, et al. 3d Bioprinting: Printing Parts for Bodies. Vol. 1566. ARC Centre of Excellence for Electromaterials Science; 2014. p. 1. ISBN 978-0-646-92867-8
- [15] Dawood A, Marti BM, Sauret-Jackson V, et al. 3d printing in dentistry. *British Dental Journal*. 2015;**219**(11):521
- [16] Zhu W, Qu X, Zhu J, et al. Direct 3d bioprinting of prevascularized tissue constructs with complex microarchitecture. *Biomaterials*. 2017;**124**:106-115
- [17] Murphy SV, Atala A. 3d bioprinting of tissues and organs. *Nature Biotechnology*. 2014;**32**(8):773
- [18] Mulford JS, Babazadeh S, Mackay N. Three-dimensional printing in orthopaedic surgery: Review of current and future applications. *ANZ Journal of Surgery*. 2016;**86**(9):648-653

- [19] Samset E, Schmalstieg D, Vander Sloten J, et al. Augmented Reality in Surgical Procedures. *Human Vision and Electronic Imaging XIII* ; 2008. p. 68060K
- [20] Modabber A, Ayoub N, Bock A, et al. Medial approach for minimally-invasive harvesting of a deep circumflex iliac artery flap for reconstruction of the jaw using virtual surgical planning and cad/cam technology. *British Journal of Oral and Maxillofacial Surgery*. 2017;**55**(9):946-951
- [21] Guo HC, Wang Y, Dai J, et al. Application of 3d printing in the surgical planning of hypertrophic obstructive cardiomyopathy and physician-patient communication: A preliminary study. *Journal of Thoracic Disease*. 2018;**10**(2):867
- [22] Starosolski ZA, Kan JH, Rosenfeld SD, et al. Application of 3-d printing (rapid prototyping) for creating physical models of pediatric orthopedic disorders. *Pediatric Radiology*. 2014;**44**(2):216-221
- [23] Flügge TV, Nelson K, Schmelzeisen R, et al. Three-dimensional plotting and printing of an implant drilling guide: Simplifying guided implant surgery. *Journal of Oral and Maxillofacial Surgery*. 2013;**71**(8):1340-1346
- [24] Egger J, Kapur T, Fedorov A, et al. GBM volumetry using the 3d slicer medical image computing platform. *Scientific Reports*. 2013;**3**:1364
- [25] Egger J, Gall M, Tax A, et al. Interactive reconstructions of cranial 3d implants under mevislab as an alternative to commercial planning software. *PLoS One*. 2017;**12**(3):e0172694
- [26] Deeley MA, Chen A, Datteri R, et al. Comparison of manual and automatic segmentation methods for brain structures in the presence of space-occupying lesions: A multi-expert study. *Physics in Medicine & Biology*. 2011;**56**(14):4557
- [27] Taha AA, Hanbury A. An efficient algorithm for calculating the exact hausdorff distance. *IEEE Transactions on Pattern Analysis and Machine Intelligence*. 2015;**37**(11):2153-2163
- [28] Bulbul A, Capin T, Lavoué G, et al. Assessing visual quality of 3-d polygonal models. *IEEE Signal Processing Magazine*. 2011;**28**(6):80-90
- [29] Cloud Compare. 2019. Available from: <https://www.cloudcompare.org/doc/qCC/CloudCompare%20v2.6.1%20-%20User%20manual.pdf> [Accessed: June 20, 2019]
- [30] Nora H. Dual energy CT as an alternative for ion radiotherapy treatment planning [doctoral dissertation]. Germany: Combined Faculties for the Natural Sciences and for Mathematics of the Ruperto-Carola University of Heidelberg; 2014
- [31] Torikoshi M, Tsunoo T, Sasaki M. Electron density measurement with dual-energy x-ray ct using synchrotron radiation. *Physics in Medicine & Biology*. 2003;**48**(5):673-685
- [32] Kemerink GJ. The nonlinear partial volume effect and computed tomography densitometry of foam and lung. *Medical Physics*. 1995;**22**(9):1445-1450